

A double-frequency dwarf nova oscillation in OY Car

T. R. Marsh¹ and Keith Horne²

¹*Department of Physics and Astronomy, University of Southampton, Highfield, Southampton SO17 1BJ*

²*School of Physics and Astronomy, University of St. Andrews, North Haugh, St. Andrews, Fife KY16 9SS*

Accepted 28 May 1998 Received ?? in original form ??

ABSTRACT

We have detected coherent oscillations (“dwarf nova oscillations”) in *Hubble Space Telescope* spectra of the dwarf nova OY Car. The oscillations were seen towards the end of a superoutburst of OY Car. The oscillations are extraordinary compared to the many other examples in the literature for two reasons. First, their amplitude is large, with a peak-to-peak variation of 8 to 20% of the total flux over the range 1100 to 2500Å. However, most remarkably we find that there are *two* components present simultaneously. Both have periods close to 18 s (equivalent to 4800 cycles/day) but they are separated by 57.7 ± 0.5 cycles/day. The lower frequency component of the pair has a strong second harmonic while its companion, which has about twice its amplitude, does not. The oscillation spectra appear hotter than the mean spectrum and approximately follow the continuum distribution of a black-body with a temperature in the range 30,000 to 50,000 K.

We tentatively suggest that the weaker non-sinusoidal component could represent the rotation of the white dwarf, although we have been unable to recover any such signal in quiescent data.

Key words: accretion, accretion discs – novae, cataclysmic variables – stars: oscillations – stars: individual: OY Car

1 INTRODUCTION

Dwarf nova oscillations (DNOs) are one of the unsolved mysteries of cataclysmic variable stars. First discovered by Warner & Robinson (1972), DNOs appear during outbursts as moderately coherent oscillations (with $Q = P/\delta P$ from 10^4 to 10^6) with periods from around 7 to 40 seconds, (although recently the lower limit has been extended to 2.8 seconds from observations of SS Cygni, van Teeseling 1997, Mauche 1997). The short periods clearly implicate the inner accretion disc and white dwarf. However while the rotation of the white dwarf is too coherent to match period changes seen in DNOs, it is hard to see how the accretion disc can produce anything as coherent as observed. The amplitudes (peak-to-peak) of DNOs in optical observations are typically less than 0.5% and therefore they can often only be detected after period analysis. The amplitudes increase towards shorter wavelengths and are tens of percents in X-ray light curves (Cordova et al. 1984). The periods of DNOs correlate with system brightness, becoming shorter as the system becomes brighter and vice versa.

DNOs seen so far have exhibited a single, sinusoidal signal (although quasi-periodic oscillations are occasionally seen as well). In this paper we present data that violates both generalisations. We will show that DNOs present in *Hubble Space Telescope* observations of the short-period

($P = 91$ min) eclipsing dwarf-nova OY Car have two components, one of which has a strong second harmonic. We begin by describing the observations.

2 OBSERVATIONS

On 24 April 1992 (pre-COSTAR) we took 419 spectra covering the range 1150 to 2510Å with the G160L grating and the Faint Object Spectrograph (FOS) on the Hubble Space Telescope. Each exposure was 4.74 s long, and the time from the start of one exposure to the start of the next was 5.60 s.

With the G160L grating, FOS also captures the zeroth order undispersed light which is weighted to longer wavelengths. The pass-band of the zeroth order light has been calibrated by Eracleous et al. (1994) who found that it has a full width at half maximum of 1900Å centred on 3400Å and who determined a scale factor of 820 counts/sec/mJy for our 4.3” aperture.

OY Car at this time was right at the end of a super-outburst which started some 17 days earlier. All amateur measurements taken after our run were upper limits, and so we believe that our data were taken within a day of the return to quiescence. Eight other *HST* observations of the outburst were made prior to those we describe here, the closest being observed two days earlier. No oscillations were

arXiv:astro-ph/9806033v1 2 Jun 1998

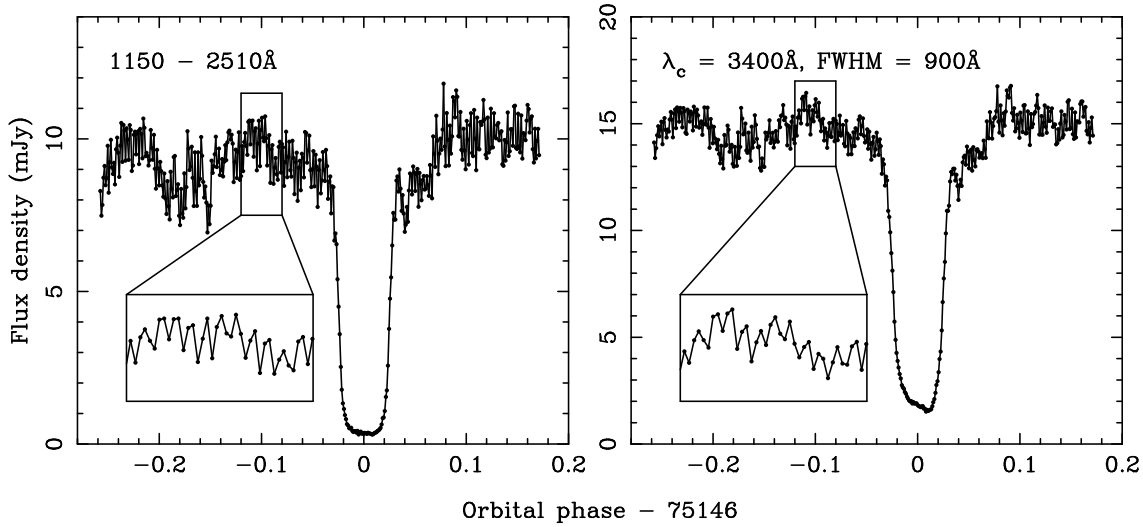


Figure 2. The light curve of OY Car in the first order dispersed light is plotted in the left panel whilst the right panel shows the zeroth order light curve. Both light curves show periodic oscillations. The oscillation is relatively stronger in the shorter wavelength (left-hand) panel.

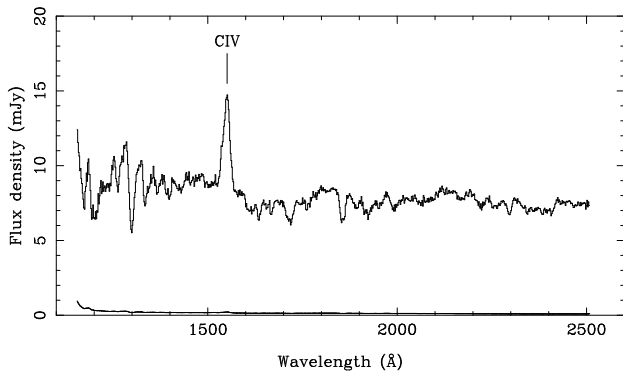


Figure 1. The mean spectrum of OY Car observed at the end of a superoutburst with the G160L grating and HST/FOS. The lower line shows the 1σ uncertainties on the spectrum.

found in any of these. Similarly, we find no oscillations in any of 7 succeeding observations during quiescence, the first of which took place 10 days after the observations reported here.

3 RESULTS

The mean spectrum during the observations is presented in Fig. 1. The spectrum is blue (note that it is plotted in terms of f_ν) with modest CIV emission. The continuum is very complex with many features from what has previously been recognised as the “iron curtain” of material that partially absorbs light from the inner disc and white dwarf (Horne et al. 1994). The broad dips around 1600 to 1800Å and beyond 2200Å are highly characteristic in this regard.

It is the light curves (Fig. 2) that prove to be unusual. As well as very deep eclipses characteristic of a small light source concentrated at the centre of the disc, they exhibit what appears at first to be a curious noise pattern. This is in fact the dwarf nova oscillation, and is a rare case in which it

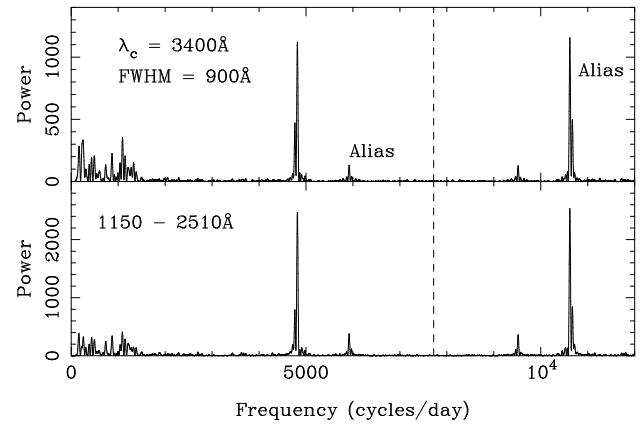


Figure 3. The Lomb-Scargle periodograms of the two orders are plotted beyond the Nyquist frequency (dashed line). The peak at 5900 cycles/day is an alias of the second harmonic (seen near 9500 cycles/day) of the component near 4800 cycles/day.

can be seen directly in the raw data. The mean flux level of around 9 mJy compares to a level of about 1 mJy observed during quiescence.

The periodogram (Lomb 1976; Scargle 1982) of each light curve is shown in Fig. 3. These were computed after masking out data affected by the eclipse and then fitting and subtracting a 7th order polynomial from the data to remove long timescale variations. At high frequencies, the periodograms are dominated by two peaks close to 4800 and 5900 cycles/day respectively. We will show below that the lower frequency “peak” is composed of two closely spaced signals. After some time we realised that the higher frequency peak is the alias of a peak near 9500 cycles/day as we show in Fig. 3 by extending it beyond the Nyquist frequency (7719 cycles/day). We make this identification because, as we will show, the 9500 cycles/day peak is then the second harmonic of the *weaker and lower frequency* component of the 4800 peak. The aliasing is a consequence of the length of

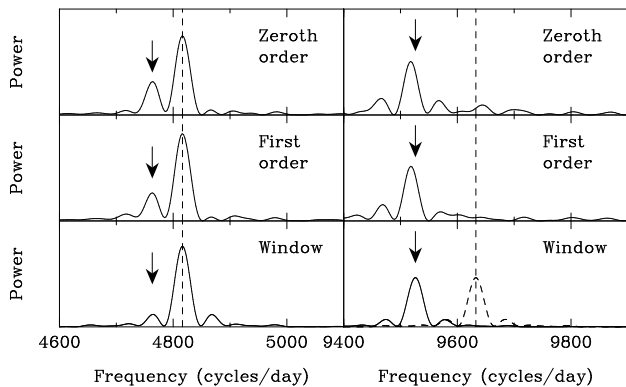


Figure 4. The figure shows regions around the two main peaks of the periodogram of Fig. 3. In the left-hand panels the peak marked with an arrow is stronger in the data than in the window function (generated by replacing the data with a pure sinusoid). On the right, the arrows indicate the expected position of the second harmonic of the peak marked by an arrow in the left-hand panels. There is no sign of a second harmonic of the stronger peak of the left-hand panel.

our exposures, which have the additional effect of reducing the amplitude of the signal. If a signal of period P is sampled with exposures of length Δt , then the observed amplitude is $\sin(\theta)/\theta$ times the true amplitude where $\theta = \pi\Delta t/P$. In our case $\Delta t = 4.74$ s, whereas 9500 cycles/day corresponds to $P = 9.09$ s, leading to a reduction factor of 0.61. In the periodogram, this is squared and means that the peak at 6000 cycles/day is only 37% of its true height. For the same reason, the third harmonic is reduced to only 7% of its true height. Unfortunately the aliasing means that the third harmonic is expected to be at 1160 cycles/day in a region of high background from low frequency power, and it cannot be detected.

We said above that the main peak has two components the weaker of which has a second harmonic. This is shown in Fig. 4 where we isolate the two peaks at 4800 cycles/day and the second harmonic at 9500 cycles/day. We also display “window” functions computed by replacing the data by pure sinusoids, including the mask around eclipse. In the left-hand series of panels, the data show a peak immediately to the left of the main peak which is not seen as strongly in the window function. The strongest peak is at 4816.32 cycles/day while its companion is some 53 cycles/day lower at 4763.12. Unfortunately because of the short length of our observation, there is a weak peak at the same place in the window function and on this basis alone we would be hesitant in claiming the presence of two signals. However in the right-hand panels, we see the second harmonic of the 4763 component while there is no detectable second harmonic of its stronger companion. This shows that the component indicated by an arrow in the left-hand panels of Fig. 4 is not merely an artefact of sampling.

The Lomb-Scargle periodogram is not really appropriate in cases where more than one frequency is present, although if they are far enough apart we would not expect significant problems in determining the frequencies of the peaks. In this case however, two frequencies are close, and there must be doubt over the accuracy of the numbers quoted above. On the other hand, we need to know them

Table 1. Frequencies of components

Lomb-Scargle ^a	1 cpt	Bayesian models	
		3 cpt	2 cpt ($f_3 = 2f_2$)
4816.32	4816.26 ± 0.27	4816.59 ± 0.34	4816.72 ± 0.31
4763.12	4763.19 ± 0.42	4760.13 ± 1.21	4759.05 ± 0.33
9518.41	9518.36 ± 0.65	9517.94 ± 0.68	9518.10 ± 0.66

^a The frequencies are all measured in units of cycles/day

accurately in order to verify quantitatively our identification of the second harmonic. That this is a significant problem is seen once uncertainties are placed on the frequencies. Using Bayesian probability theory (as outlined in the appendix) it is straightforward to extend the periodogram to account for any number of periodic components. For a single component, this reduces to a form very close to the Lomb-Scargle version, and shows that the periodogram is closely related to the natural log of the posterior probability distribution of the period. The curvature then gives the uncertainty, and applying this we obtain the frequencies of the three main peaks listed in the second column of Table 1, which can be compared to the values obtained from the Lomb-Scargle periodogram listed in the first column. As expected the values in the first two columns of table 1 are almost identical, but now with uncertainties we can compare the frequencies of the peaks at $f_2 = 4763$ and $f_3 = 9518$ cycles/day that we claim are harmonically related to each other. We find the difference $2f_2 - f_3 = 8.02 \pm 1.06$ cycles/day, and it would seem that there is a problem. This is the reason why in Fig. 4 the predicted second harmonic indicated by the arrow in the right-hand panels is not a perfect match to the observed peak. However, once three components are included correctly (see the appendix), we obtain the values in the third column. The frequencies do indeed change, and now the difference between the harmonically related components becomes $2f_2 - f_3 = 2.32 \pm 1.39$, in acceptable agreement within the uncertainties. Given the harmonic relation, we can re-fit the frequencies on the basis that $f_3 = 2f_2$ exactly, so that there are only 2 independent frequencies, and we arrive at the fourth column which contains the final values that we will use from now on. It can be seen that it is the harmonic at 9518 cycles/day which dominates the determination of the frequency, and as we will show, it has a higher amplitude than the fundamental.

The referee has pointed out that a single component with a phase and/or period change might appear as more than one period in periodograms, and that just such changes have been observed in other examples of DNOs. This is certainly true. We carried out some tests with a single signal of constant period suffering a sharp phase shift about half way through the observations. As the phase shift increases, one of the two side peaks grows in strength while the main peak shifts in frequency and weakens. When the phase shift reaches about 120° the periodogram appears not unlike Fig. 4. In this case the “true” frequency is placed somewhere between the two peaks, but is closest to the strongest peak. The coincidence of the weaker peak (the f_2 component) with one of the two side-lobes of the f_1 component is suspicious in this regard. We reject this possibility however because of the f_3 component which agrees to within 1.7σ of $2f_2$ and

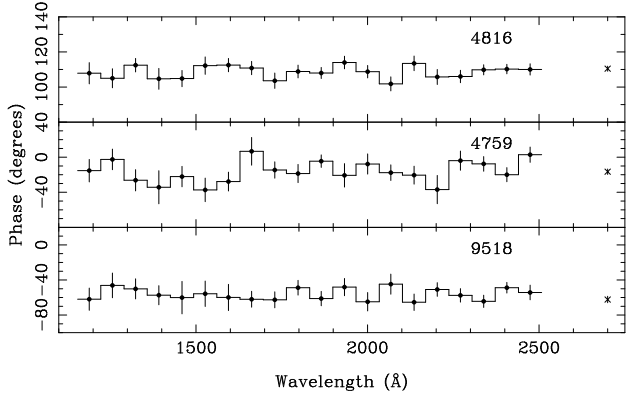


Figure 5. The phases of the 3 components of the oscillations are plotted versus wavelength. The right-most point is the phase of the zeroth order light curve. There is no evidence for any dependence of phase upon wavelength. The phases are measured with respect to the zero point $HJD = 2448736.835$.

yet is 120σ away from $2f_1$. This means that f_3 is the second harmonic of f_2 , and thus component f_2 is genuinely independent of f_1 . We further note that while we know of no other multiply periodic DNOs, multiple periodicity has been seen in the dwarf nova WZ Sge in quiescence (Patterson et al. 1998).

3.1 Spectra of the oscillations

Armed with accurate frequencies for the three components (two of them harmonically related), we can fit sinusoids at many different wavelengths to obtain the spectra of the oscillations. To do so we fit all three components simultaneously to the spectra, using the form $a \cos 2\pi ft + b \sin 2\pi ft$ for each component. This can be re-expressed as $A \cos 2\pi(ft + \phi)$ where the semi-amplitude $A = \sqrt{a^2 + b^2}$ and the phase ϕ is given by $\tan 2\pi\phi = -b/a$. The estimate of amplitude A suffers from a noise bias (it can only be positive). Although this can be corrected approximately, it is preferable to see first if there is any evidence for a variation of phase with wavelength. If not, then ϕ can be fixed and we can derive an unbiased estimate of the semi-amplitude. The phase versus wavelength is plotted in Fig. 5 and shows that the phase is indeed independent of wavelength in all three components. The weighted mean phases of both orders was then computed in order to fit the amplitudes. We obtain the values $110.6^\circ \pm 0.8$, $-15.4^\circ \pm 1.9$ and $-57.7^\circ \pm 1.9$ for the 4816, 4759 and 9518 components respectively. The latter two values show that the 9518 harmonic peaks $13.9^\circ \pm 2.1$ after the 4759 fundamental, as measured in terms of the fundamental's phase.

Holding the phases fixed we then fitted the amplitudes which are plotted Fig. 6. The oscillation spectra show no sign of the CIV emission seen in the mean spectrum (at 1550\AA). The CIV is thought to form by scattering of continuum photons in an outflow above and below the disc. It therefore gives us an angle-integrated view of the inner disc brightness. This suggests that the oscillations are not produced by the entire luminosity of the system varying, but rather by the varying visibility of some hot source. This counts

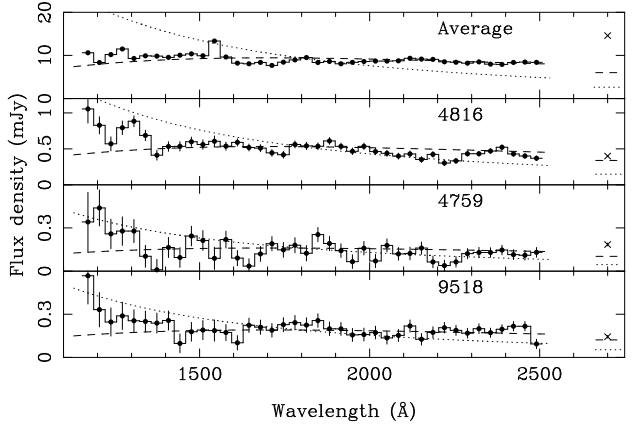


Figure 6. The semi-amplitudes of the 3 components of the oscillations are plotted versus wavelength along with the mean spectrum binned to the same scale. The right-most point is the zeroth order point scaled according to the calibration of Eracleous et al. (1994) and shifted in wavelength to avoid compressing the first order spectrum; while the statistical uncertainties on these points are low there is a 50% uncertainty in their calibration which would move them all up or down by the same factor. The dashed lines show black-body spectra for $T = 30,000$ K, while the dotted lines are Rayleigh-Jeans spectra. The values plotted are not corrected for the amplitude reduction caused by the finite length exposures.

against radial oscillation models such as those of Molteni et al. (1996).

The oscillation spectra are very much hotter than the average spectrum. This can be seen over the range of the first order dispersed light but more clearly still in the ratio of first to zeroth order light. This agrees with earlier work at optical wavelengths (e.g. Middleditch & Cordova 1982; Stiening et al. 1984); our data extend this result into the space ultraviolet. Partly as a result, the peak-to-peak amplitude in the first order light is very high, reaching almost 20% at the shortest wavelengths of the 4816 component. In the zeroth order light, this has fallen to 5%. Schoembs (1986) observed a maximum amplitude of 2.2%, but given that his observations were approximately B band (our zeroth order has a central wavelength of 3400\AA) and the very blue spectra, our values are probably comparable.

The spectra of DNO are so blue that ground-based data can only put a lower limit upon their temperature. With our coverage of the ultraviolet we might hope to fare better. Indeed, the Rayleigh-Jeans spectra plotted in Fig. 6 are hotter than any of the oscillation spectra, particularly in the small amount of zeroth order flux they produce. Allowing for the 50% uncertainty Eracleous et al. (1994) quote on their calibration of the zeroth order flux, we deduce an upper limit of about 50,000 K if the oscillation spectra are black-bodies. The lower limit is independent of the zeroth order calibration since it is fixed by the short wavelength ultraviolet flux. We place a lower limit of about 30,000 K (see Fig. 6) from such a comparison.

The ratios of the oscillation amplitude in the first order light divided by its amplitude in zeroth order (both measured in counts/sec) are 1.37 ± 0.04 , 1.10 ± 0.08 and 1.53 ± 0.11 for the 4816, 4759 and 9518 components respectively; the ratio of the mean fluxes in each order is 0.68. Thus the second harmonic 9518 component is hotter than its fundamental

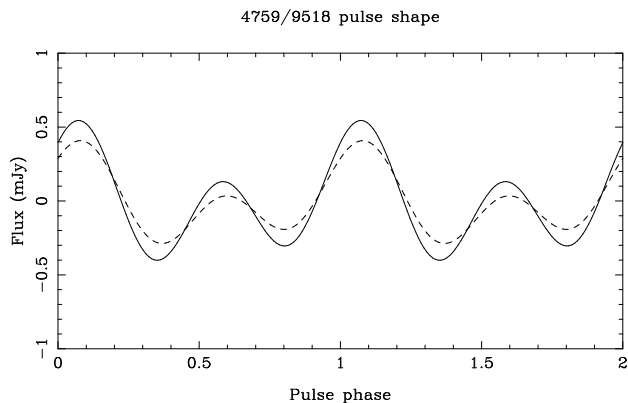


Figure 7. The shape of the 4759/9518 obtained from sinusoid fits and corrected for the amplitude reduction caused by the finite exposure lengths. The solid and dashed lines represent the first and zeroth orders respectively. The pulse phase is measured in terms of the 4759 fundamental with respect to the zero point $HJD = 2448736.835$.

counterpart at 4759 cycles/day. Moreover, the amplitude of the second harmonic is larger than the fundamental. We find the ratios of the 9518 to 4759 amplitudes (corrected for the finite exposure factor discussed earlier) to be 1.58 ± 0.09 in the first order and 1.14 ± 0.09 in the zeroth order. Along with the phases mentioned earlier, these lead to the pulse shapes shown in Fig. 7. This plot shows a significant “interpulse” which will be of significance in the discussion section. The true pulse shape may be more complex since our exposures were too long to detect any but the first two harmonics.

3.2 The eclipse of the oscillations

As OY Car is eclipsing, we can learn something about the distribution of the oscillating light by measuring the amplitude and phase of the oscillations as a function of time. The standard method of doing so is to hold the period fixed and then fit sinusoids to short sections of the data. How short a section can be used depends upon the strength of the oscillations. Our oscillations are especially strong, but we have the extra complication of multiple periods. While it is almost as easy to fit to several periods as it is to fit to one, the solutions become ill-conditioned if data segments are not long enough to separate the periods. This is most obviously a problem with the 4816 and 4759 components which can only barely be separated using all of our data. Therefore for the purposes of this section we simply ignore the weaker component (4759) while realising that it will cause a certain amount of interference or “beating”. Unfortunately spectral leakage from the 4816 component can also affect the 9518 component, which since it appears at 5900 cycles/day because of aliasing is much closer than it seems. We applied a linear taper to the data segments in an effort to reduce the leakage, but were forced to use segments of 30 points each for the 9518 component. For the 4816/4759 combination we settled on 16 points per segment, and in each case we used a 50% overlap from one segment to the next. Prior to splitting the data up we also applied a high-pass filter to remove low frequencies in order to prevent leakage from them affecting

the results. The results of the fits are shown in Figs. 8 and 9 for the first and zeroth order light respectively.

In interpreting the plots it should be remembered that the amplitude measurements are subject to a positive bias of the same order as the uncertainties plotted and so the amplitudes during eclipse are consistent with no detection even though it appears that with several marginal detections there is some evidence for oscillations during eclipse. Both the mean flux and oscillations are deeply eclipsed, but from the zeroth order results on the 4816 component in Fig. 9 we can say that the oscillations are even more deeply eclipsed than is the mean light. The other panels give no clear answer, partly because the eclipse is very deep even in the mean light, and partly because of the noise bias discussed earlier.

Since we know that the period of the oscillations imply an origin in the inner disc or white dwarf, it may not seem that we have learned much. However, in other systems, such as DQ Her and UX UMa, the oscillating light is spread out, indicating that we see light reprocessed from the disc. Phase shifts observed during eclipse show where the reprocessing occurs (Petterson 1980). It seems then that such effects play at best a minor role in our data; we will look at reprocessing in more detail in section 4.1.

4 DISCUSSION

Our *HST* data are qualitatively different from previous observations of dwarf nova oscillations. The essential features of our data are (a) the simultaneous presence of two oscillations each with a period close to 18s but separated by 57.7 ± 0.5 cycles/day, and (b) a strong second harmonic of the weaker and lower frequency component which peaks just 13° after the fundamental, and no second harmonic of the stronger component.

To our knowledge, there are no previous cases of either multiple or non-sinusoidal oscillations. As has long been realised, the short periods of DNO imply an origin in or near the white dwarf. The direct interpretation of our data is that this region is capable of producing two oscillations of different character at the same time. Although it is not clear why it has not been seen before, it is what we believe is happening. However, before proceeding upon this basis, we will first consider an attractive alternative which turns out not to be satisfactory.

4.1 Reprocessing models

We already know of one class of cataclysmic variable star in which a signal at one period can give rise to others. These are the DQ Her stars in which a coherent signal from the rotation of a magnetic white dwarf can be detected. These stars also show sidebands to the rotation frequency displaced by the orbital frequency. Such sidebands can result from modulation of the spin frequency ω on the orbital frequency Ω which leads to $\omega \pm \Omega$ sidebands. A single sideband at $\omega - \Omega$ can result from reprocessing of the spin pulses off structures fixed in the rotating frame or from direct interaction of the gas stream with the magnetosphere of the white dwarf. It is clear then that such effects are possible, but could they be occurring in OY Car?

The DQ Her analogy suggests that the 4759 cycles/day

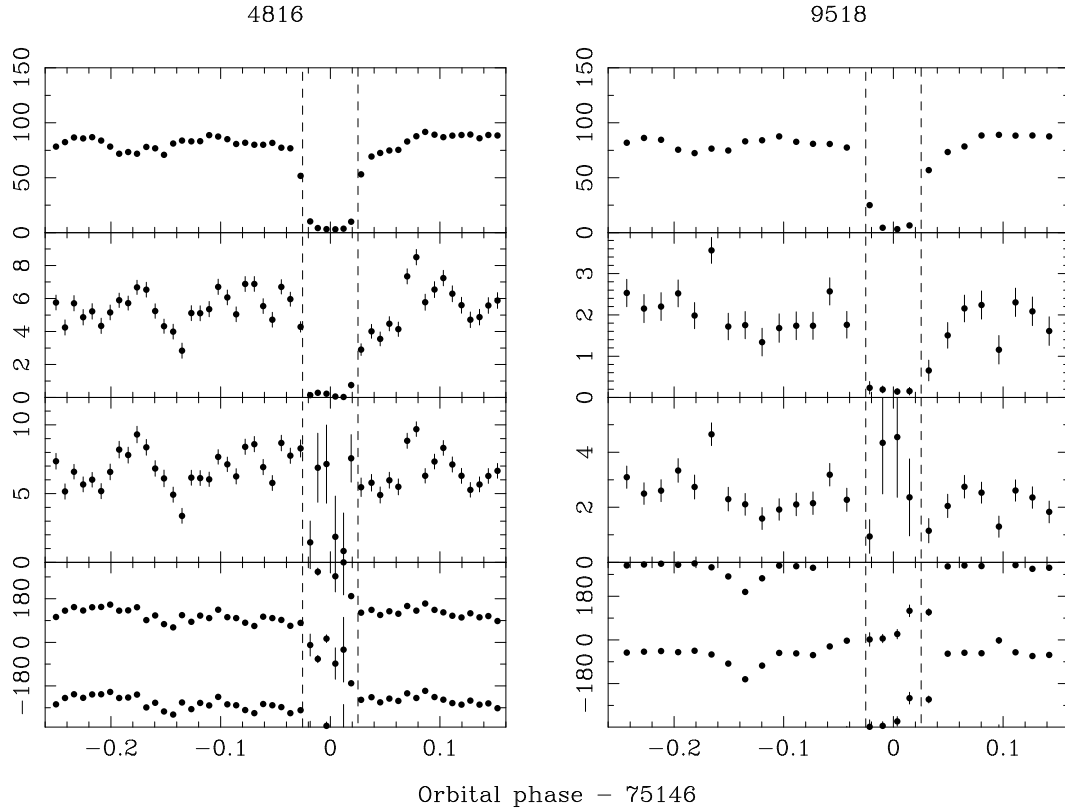


Figure 8. From the top are plotted the mean flux, oscillation amplitude, percentage oscillation amplitude and oscillation phase (degrees) evaluated over data segments of 16 points for the 4816 component and 30 for the 9518 component for the first order light.

component might be a sideband of the 4816 component. We expect it to be this way round because the 4816 component is the stronger and because if the light source and reprocessing structure orbit in the same direction, the reprocessed frequency is lower than the main signal. In addition the 4816 component is sinusoidal and thus can be identified with the “standard” DNO of other observations. The reprocessing structure must advance in the inertial frame at the 57.7 ± 0.5 cycles/day splitting we measured earlier. This is 3.6 ± 0.03 times the orbital frequency in OY Car. During superoutburst it is thought that the accretion disc reaches a radius where it orbits 3 times for each orbit of the binary (Whitehurst 1988). The 3:1 resonance then drives the disc into an eccentric shape and subsequent precession can then explain the observation of flares or “superhumps” on periods longer than the binary period. From Kepler’s third law, a ratio of 3.6 corresponds to a radius of about 89% of the 3:1 radius. Since our observations were placed right at the end of outburst when the disc should have shrunk somewhat, this seems plausible. There are many other constraints that such a model must satisfy however.

First of all there must be an asymmetry in the outer disc so that we can see it lit up every time the beacon from the inner disc sweeps by it. One cannot expect any such asymmetry to last very long since shear in the disc always tends to smear out azimuthal structure. While we cannot suggest a mechanism for generating such an asymmetry, its short-lived nature could be viewed as a plus point since then such extra components would be rarely seen. In order to be

consistent with the eclipse results, we also have to suppose that the asymmetry is small enough to be totally eclipsed.

Even allowing the above constraints, there are higher hurdles for reprocessing models to face. The blue colours of the oscillation spectra imply a high effective temperature, particularly so since our spectra extend into the space ultraviolet. A comparison of the zeroth to first order flux ratio with black-body models of reprocessing suggest an effective temperature of at least 20,000 K. This is lower than the 30,000 K limit discussed earlier because oscillation spectra can appear more blue than the source of light that produces them since they depend upon the derivative of the spectrum with respect to temperature. The luminosity L needed to produce reprocessed radiation with effective temperature T_{eff} at radius R in the disc is given by

$$L = 4\pi R^2 \sigma T_{\text{eff}}^4 \frac{d \ln R}{d(H/R)},$$

where H is the scale height in the disc. Taking $H/R \propto R^\beta$, then the derivative term becomes $1/(\beta H/R)$. Typically $\beta \sim 1/8$ (Shakura & Sunyaev 1973) and we take $H/R \sim 1/20$ and so the derivative term is of order 160.

Taking Wood & Horne’s (1990) parameters for OY Car, the 3.6:1 radius corresponds to $R = 0.41a$ or 1.9×10^8 m. We then find that to reach our minimum of 20,000 K the central peak luminosity must be of order $L = 1700 L_\odot$. The accretion luminosity of the inner disc and boundary layer, $G\dot{M}/R$, set an upper limit to the mean luminosity of the oscillating source (which is half the peak luminosity assuming 100% modulation). We find $\dot{M} > 3 \times 10^{-7} M_\odot/\text{yr}$, which

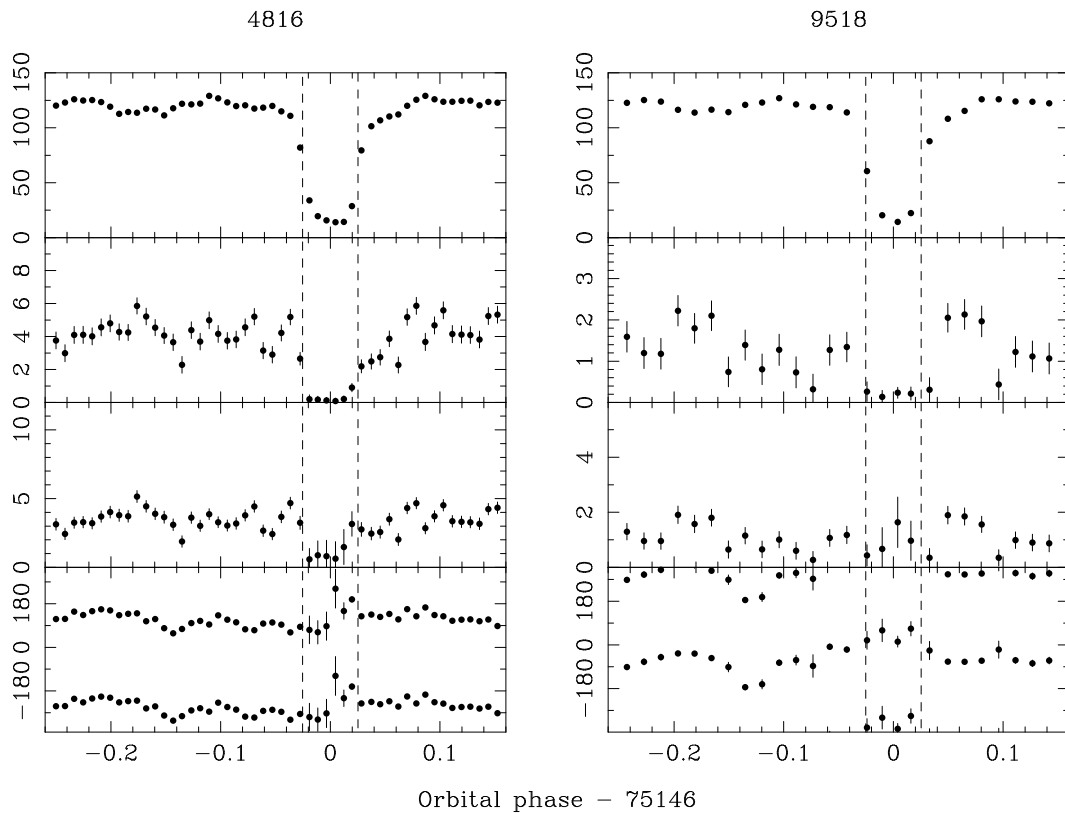


Figure 9. From the top are plotted the mean flux, oscillation amplitude, percentage oscillation amplitude and oscillation phase (degrees) evaluated over data segments of 16 points for the 4816 component and 30 for the 9518 component for the zeroth order light.

is higher than the maximum rate expected for dwarf novae, and a strong point against reprocessing.

The second harmonic is perhaps even more difficult to understand on the reprocessing model. It requires a non-linear reponse to the incident flux and can be generated if as the flux incident on the disc rises, the reprocessing efficiency rises as well, thus sharpening the peaks. However even if this process is taken to its extreme to produce a series of sharp spikes or delta-functions, we can only obtain a second harmonic equal to the fundamental. In our case the second harmonic is stronger than the fundamental by a factor of 1.58 ± 0.09 in the first order light and 1.14 ± 0.09 in the zeroth order as illustrated in Fig. 7. In order to obtain the pulse shapes seen one is forced to suppose a complex response in which the reprocessing efficiency at first decreases and then increases with rising incident flux. We find this very implausible.

Our conclusion is that a single oscillation plus reprocessing cannot explain our observations: there really are two oscillations present at the same time.

4.2 Two oscillations

Accepting that both oscillations are generated on or near the white dwarf, how do they originate? The trapped g - and r -mode model of Papaloizou & Pringle (1978) can certainly produce more than one oscillation frequency. Indeed, it is hard to see how this model could only produce one frequency, an argument that has been used in the past against it. Now we have seen more than one component. However, in

our view this does not support Papaloizou & Pringle’s model because each component has a very different character, and if two oscillations are possible, why not more?

Another model of DNOs frequently discussed is one in which the DNO frequency represents the keplerian orbital frequency of some part of the inner disc (Bath 1973; Mauche 1996). On this model for instance, the 4816 component might represent the keplerian frequency, and, if so, it corresponds to an orbital radius of 1.4 times the radius of the white dwarf on the physical parameters of Wood & Horne (1990). Explaining the relatively high coherence of DNOs has always seemed difficult for keplerian models as why should just one specific orbital frequency dominate? Our data perhaps provide some support however because there is an appealing explanation for the 4759/9518 combination, which might represent either the white dwarf rotation frequency or the beat frequency between the white dwarf and keplerian frequencies. In the latter case the white dwarf would rotate at the frequency difference of 57.7 ± 0.5 cycles/day. An attractive feature of this model is that it is entirely natural that the two components should have a different nature and second harmonics are easily produced if the white dwarf has two accreting poles for instance. Given a choice between 4759 or 57.7 cycles/day for the rotation frequency of the white dwarf, we would favour 4759 since we already know of short rotation period examples such as AE Aqr and DQ Her, amongst weakly magnetic accretors, a category which OY Car surely falls into. On the contrary, it is hard to imagine how the white dwarf in OY Car could have the 25 minute period required to match the 57.7 fre-

quency splitting as this would be longer than in many of the longer period DQ Her stars. On the basis of this idea, we searched for coherent periodicities in 7 epochs of *HST* taken during quiescence following the outburst and in Wood et al.'s (1989) ground-based photometry. We failed to find any coherent signals, with detection levels of 0.1 and 0.3% respectively (these limits only apply above 1000 cycles/day, because orbital variations and flickering limit the sensitivity at low frequencies). In this respect at least the 4759/9518 component behaves like other DNOs which have never been seen in quiescence.

It is not clear how much the failure to detect the 4759/9518 component in quiescence counts against its being the rotation frequency of the white dwarf. We speculate that perhaps it only becomes evident when the inner disc orbital period (represented by the 4816 component) is close to co-rotation with the white dwarf (4759 component). Such a situation may favour the largest difference between accretion rate onto the poles compared with other parts of the white dwarf making the white dwarf spin period detectable. We note that the shortest DNO period from OY Car observed by Schoembs (1986) of 19.44 seconds is over 300 cycles/day away from 4759 and may have already been too different to generate the 4759/9518 signal.

A third, hybrid model has been put forward by Warner (1995), based upon an earlier model of Paczynski (1978). In this model the DNO frequency is set by the outer layers of a weakly magnetic white dwarf decoupling from the white dwarf itself. The variation in period is put down to the spin up/down of the layer with accretion rate. This model suffers from the same problem as the keplerian models in that it is hard to see how a coherent oscillation can result. Now with our data, there is an additional difficulty as Warner's model does not appear to have any natural means for producing more than one periodicity.

In summary while none of the current models provide a convincing explanation for DNOs, our observation of two components seems more naturally explained by keplerian orbit models than any other.

5 CONCLUSIONS

We have found dwarf nova oscillations at the end of a super-outburst observed with *HST*. The oscillations have a large amplitude, reaching 20% peak to peak at the shortest ultraviolet wavelengths. Most remarkably there are two oscillations present with similar periods, and the weaker and longer period of the two has a strong second harmonic.

We discuss several current models and while none are persuasive, models in which the DNO frequency represents an orbital frequency of the inner disc give the most natural explanation of the additional component as it can represent the rotation of the white dwarf. However, we have been unable to find any sign of such a component during quiescence, and so, if our suggestion is true, some means of suppressing the signal is required.

ACKNOWLEDGMENTS

TRM was supported by a PPARC Advanced Fellowship during the course of this work. The data reduction and analysis were carried out on the Southampton node of the UK STAR-LINK computer network. We are grateful to Janet Wood for making her ground-based photometry available to us.

REFERENCES

- Bath, G., 1973, *Nature Phys. Sci.* 246, 84.
 Bretthorst, G.L., 1988, *Bayesian Spectral Analysis and Parameter Estimation*, (New York: Springer)
 Cordova, F.A., Chester, T.J., Mason, K.O., Kahn, S.M., Garmire, G.P., 1984, *ApJ*, 278, 739.
 Eracleous, M., Horne, K., Robinson, E.L., Zhang, E.-H., Marsh, T.R., Wood, J.H., 1994, *ApJ*, 433, 313.
 Gregory, P.C., Loredo, T.J., 1992, *ApJ*, 398, 146
 Horne, K., Marsh, T.R., Cheng, F.-H., Hubeny, I., Lanz, T., 1994, *ApJ*, 426, 294.
 Lomb, N.R., 1976, *Ap&SpSci*, 39, 447.
 Mauche, C.W., 1996, *ApJ*, 463, L87.
 Mauche, C.W., 1997, in *13th North American Workshop on Cataclysmic Variables*, ed. S.Howell, E.Kuulkers and C.Woodward, (San Francisco: ASP), in press.
 Molteni, D., Sponholz, H., Chakrabarti, S.K., 1996, *ApJ*, 457, 805.
 Middleditch, J., Cordova, F.A., 1982, *ApJ*, 255, 585.
 Paczynski, B., 1978, in *Nonstationary Evolution of Close Binaries*, p89, ed. Zytkov, A., (Warsaw)
 Papaloizou, J., Pringle, J., 1978, *MNRAS*, 182, 423.
 Patterson, J., Richman, H., Kemp, J., Mukai, K., 1998, *PASP*, 110, 403.
 Petterson, J., 1980, *ApJ*, 241, 247.
 Scargle, J., 1982, *ApJ*, 263, 835.
 Schoembs, R., 1986, *A&A*, 158, 233.
 Shakura, N.I., Sunyaev, R.A., 1973, *A&A*, 24, 337.
 Stiening, R.F., Dragovan, M., Hildebrand, R.H., 1984, *PASP*, 94, 672.
 Warner, B., Robinson, E.L., 1972, *Nature Phys. Sci.*, 1972, 239, 2.
 Warner, B., 1995, *Cataclysmic Variable Stars*, CUP.
 Whitehurst, R., 1988, *MNRAS*, 232, 35.
 Wood, J.H., Horne, K., Berriman, G., Wade, R.A., 1989, *ApJ*, 341, 974.
 Wood, J.H., Horne, K., 1990, *MNRAS*, 242, 606.
 van Teeseling, A., 1997, *A&A*, 324, L73.

APPENDIX A: BAYESIAN PERIOD MEASUREMENT

The detection and measurement of periodic components can be handled using Bayesian probability theory (e.g. Gregory & Loredo 1992; Bretthorst, 1988). We consider the probability that our data is consistent with zero (model Z) versus the probability that it can be represented by a sum of N sinusoids (model S). In practice, these models imply that data must be “de-trended” by fitting polynomials or splines to remove low frequency variability prior to analysis.

We wish to compute the probability ratio of these models given the data, $P(S|D)/P(Z|D)$. Let the flux at time t_i be y_i , with uncertainty σ_i , for $i = 1$ to M . Our sinusoid can be represented in linear form as

$$y'_i = \sum_{j=1}^{2N} x_{i,j} a_j,$$

where the $x_{i,j}$ functions are alternately the value of cosine or sine evaluated for frequency j at t_i . Thus $x_{i,1} = \cos 2\pi f_1 t_i$, $x_{i,2} = \sin 2\pi f_1 t_i$, $x_{i,3} = \cos 2\pi f_2 t_i$, etc. Written in this fashion rather than with phases makes later integrations simpler.

Bayes' theorem gives

$$\frac{P(S|D)}{P(Z|D)} = \frac{P(S)}{P(Z)} \frac{P(D|S)}{P(D|Z)}.$$

The first term on the right expresses one's prior belief in each model. It is important when one is discussing whether a component is really present, but since it remains constant, it does affect the periods measured. Information about the periods is contained in the second term, which is the ratio of the probability of our obtaining the data given the models.

Let us first consider $P(D|Z)$. We assume that the data are gaussian random variables then

$$P(D|Z) = \frac{1}{\prod_{i=1}^M \sqrt{2\pi}\sigma_i} \exp \left\{ - \sum_{i=1}^M \frac{y_i^2}{2\sigma_i^2} \right\}.$$

The probability of the data given the sinusoid model is more complicated because we first need to compute it for a specific vector of parameters, i.e. $P(D|S, \mathbf{a})$. This is straightforwardly

$$P(D|S, \mathbf{a}) = \frac{1}{\prod_{i=1}^M \sqrt{2\pi}\sigma_i} \exp \left\{ - \sum_{i=1}^M \frac{(y_i - y'_i)^2}{2\sigma_i^2} \right\}.$$

In order to obtain the probability we want, $P(D|S)$, we must integrate over the parameters \mathbf{a} :

$$P(D|S) = \int \int \int \dots \int P(D|S, \mathbf{a}) P(\mathbf{a}) d\mathbf{a}.$$

Once again $P(\mathbf{a})$ is a prior probability, in this case of the semi-amplitudes. We take the amplitudes to have independent, uniform distributions over the range $-R/2$ to $+R/2$ so

$$P(\mathbf{a}) = \frac{1}{R^{2N}}.$$

One normally has little idea of what R would be, so it should be set conservatively. For example, setting R equal to the brightest OY Car has ever been seen would be a reasonable course to take. Its value has some effect on the significance of a peak but not on the value of the period deduced.

With these assumptions we now need to integrate the exponential over a $2N$ dimensional cube of side R . To make this simpler we assume that this cube contains all the region over which the exponential is significant. After some algebra we obtain

$$P(D|S) = \frac{1}{\prod_{i=1}^M \sqrt{2\pi}\sigma_i} \exp \left\{ - \sum_{i=1}^M \frac{y_i^2}{2\sigma_i^2} \right\} \times \left(\frac{\sqrt{2\pi}}{R} \right)^{2N} \frac{1}{\sqrt{\det \mathbf{X}}} \exp \left\{ \frac{1}{2} \mathbf{b}^t \mathbf{X}^{-1} \mathbf{b} \right\},$$

where the vector \mathbf{b} is given by

$$\mathbf{b} = \begin{pmatrix} \sum_i w_i x_{i,1} \\ \sum_i w_i x_{i,2} \\ \vdots \\ \sum_i w_i x_{i,2N} \end{pmatrix}$$

and the $2N$ by $2N$ symmetric matrix \mathbf{X} is given by

$$\mathbf{X} = \begin{pmatrix} \sum_i w_i x_{i,1} x_{i,1} & \dots & \sum_i w_i x_{i,1} x_{i,2N} \\ \sum_i w_i x_{i,2} x_{i,1} & \dots & \sum_i w_i x_{i,2} x_{i,2N} \\ \vdots & & \vdots \\ \sum_i w_i x_{i,2N} x_{i,1} & \dots & \sum_i w_i x_{i,2N} x_{i,2N} \end{pmatrix}$$

where $w_i = 1/\sigma_i^2$ and the sums extend from $i = 1$ to M , the number of data points.

Finally dividing by $P(D|Z)$ and taking the natural logarithm we obtain

$$\ln \frac{P(D|S)}{P(D|Z)} = 2N \ln \frac{\sqrt{2\pi}}{R} - \frac{1}{2} \ln(\det \mathbf{X}) + \frac{1}{2} \mathbf{b}^t \mathbf{X}^{-1} \mathbf{b}. \quad (\text{A1})$$

Together the first two factors represent the ratio of the volume of parameter space allowed by the data compared to the volume (R^{2N}) allowed by the prior model of the semi-amplitudes. This is a factor penalising the sinusoid model for its adjustable parameters. The last factor is the important one. For example, if we take a single sinusoid model with uniform uncertainty values, one can show that the value of $\mathbf{b}^t \mathbf{X}^{-1} \mathbf{b}/2$ is identical to the expression given by Scargle (1988) for a periodogram of unequally spaced data.

The best frequencies are those which maximise the log probability ratio of Eq. A1 (which is why R has no effect upon their values). The maximum can be located using standard techniques. If at the same time the second derivative matrix is evaluated, then uncertainties can be computed. This is the procedure we applied to derive the frequencies listed in table 1 of this paper.